Quadrupolar spin relaxation of ^{14}N in NNO in collisions with various molecules

Cynthia J. Jameson and Marc A. ter Horst[a)]
Department of Chemistry M/C-111, University of Illinois at Chicago, 845 W. Taylor, Chicago, Illinois 60607-7061

A. Keith Jameson
Department of Chemistry, Loyola University, Chicago, Illinois 60626

(Received 6 July 1998; accepted 10 September 1998)

Spin-lattice relaxation times were measured for the ^{14}N relaxation of both ^{14}N nuclei in NNO in the pure gas and in mixtures with the following buffer gases; Ar, Kr, Xe, HCl, N_2, CO, CO_2, CH_4, CF_4, and SF_6. Effective collision cross sections for molecular reorientation of NNO in collisions with these ten molecules are obtained, as a function of temperature, directly from the measured relaxation times of the end ^{14}N nucleus in the NNO molecule. © *1998 American Institute of Physics.* [S0021-9606(98)01047-2]

INTRODUCTION

In dilute gases of polyatomic molecules the phenomena which are directly related to the anisotropy of the intermolecular potential function include angular momentum alignment phenomena and effects of collisions on radiation absorption or scattering. Kinetic theory allows each of these properties to be described in terms of an effective cross section which can be calculated if the intermolecular potential function is known. Of the angular momentum alignment phenomena, nuclear spin relaxation in the gas phase offers the possibility of exploring the same potential surface with more than one probe nucleus, thus providing either redundant or additional information. Spin relaxation due to interactions of unlike pairs of molecules can be characterized nearly as precisely as relaxation due to collisions of like molecules, in contrast with other thermophysical properties. Furthermore, the factors that relate the effective cross section to the spin relaxation times are well defined, and unambiguous, with no associated normalization problems. The relaxation times associated with specific relaxation mechanisms can involve first or second rank irreducible tensors; they can be related directly to a specific effective cross section for changes in the molecular angular momentum vector. The relaxation cross sections are determined by the anisotropic part of the intermolecular potential and can be obtained via scattering theory.[1] McCourt and co-workers provide a detailed derivation of the collision cross sections related to various thermophysical properties, including nuclear magnetic resonance (NMR) spin relaxation.[2,3] One type of cross section that can be derived from NMR experiments is associated with the quadrupolar, dipole–dipole, and chemical shift anisotropy mechanisms and is closely related to (for atomic collision partners, is identical to) the cross section that can be derived from depolarized Rayleigh light scattering. Another type of cross section, associated with the spin rotation relaxation mechanism, can only be obtained from NMR relaxation, and is known to be an independent probe of the anisotropy of the potential-energy surface. Together these cross sections have been found very useful in refining the anisotropy of potential functions for H_2 with He,[4–6] H_2 with Ne,[7] H_2 with Ar,[8] N_2 with Ar[9] and N_2 with Kr.[10] In fact, even with structural information and vibrational frequencies from the high-resolution spectroscopy of the van der Waals complex, the potential-energy surface (PES) cannot be adequately specified without some anisotropy information farther up from the bottom of the well. This is the type of information that spin-relaxation cross sections provide.[9,11]

In favorable systems, effective cross sections can be obtained directly from relaxation times T_1 measured in the gas phase. We report for the first time the spin relaxation of ^{14}N nuclei in the NNO molecule in the pure gas and in binary mixtures of NNO with Ar, Kr, Xe, HCl, N_2, CO, CO_2, CH_4, CF_4, and SF_6. NNO is an important molecule in the earth's atmosphere and is used as a long-lived tracer for monitoring the mixing in the stratosphere. The same quadrupolar nuclear spin that makes it possible to determine cross sections related to the reorientation of the molecular rotational angular momentum vector from our spin-relaxation experiments makes the NNO molecule attractive for studies of weakly bound complexes. In van der Waals complexes, the quadrupolar spin provides a determination of the electric field gradient at the nucleus that serves as a useful probe of electrical perturbations resulting from the intermolecular interaction. Here too, it is expected that the electronic and geometric structure of the complex derived from the quadrupolar coupling tensor of one ^{14}N nucleus should agree with that derived from the other nitrogen nucleus. van der Waals complexes of NNO with nearly all the molecules in the set of ten we have used in this work have been observed (except for CH_4 and CF_4). Molecular beam electric resonance spectroscopy showed that the structure of the NNO–Ar complex is T-shaped.[12] High-resolution infrared (IR) spectroscopy of jet cooled systems have provided spectroscopic constants and structural param-

[a)]Present address: Department of Chemistry and Biochemistry, Northwestern University, Evanston, IL 60208-3113.

eters for NNO–CO_2,[13] NNO–CO,[14,15] NNO–N_2,[16] NNO–HCl,[17] NNO–Ar,[18,19] other NNO-rare gas,[20] and $(NNO)_2$.[21,22] Pulsed Fourier transform microwave spectroscopy of a number of isotopomers of NNO–HCl provided good comparisons with *ab initio* calculations at the Møller–Plesset second-order (MP2) level,[23] and the nuclear quadrupole hyperfine structure due to both nitrogen nuclei in NNO–Ar and NNO–CO_2 is found to support the utility of quadrupolar nuclei in extracting geometrical information in such complexes.[24,25] Other spectroscopic data such as the mean-square torque have been measured for NNO–Ar and NNO–Kr,[26,27] and recently also for NNO–Xe and NNO–CO_2,[28] and for NNO–SF_6.[29] Furthermore, rotational relaxation rates for the $J=0-1$ transitions of $^{15}N^{15}NO$ upon collisions with NNO, N_2, Ar, Kr, and Xe have been determined by pulsed microwave time domain spectroscopy, providing the pressure dependence of the population and coherence decay rates $1/T_1$ and $1/T_2$.[30] These relaxation rates also depend on the anisotropy of the potential. Therefore, the availability of spin-relaxation cross sections for the NNO molecule in collisions with the set of molecules we have used is timely and will encourage more detailed examination of the PES, not just the shape of the bottom of the well for these pairs of molecules.

This study of NNO with the same set of collision partners as we have used for CO_2[31] is also motivated by a desire to understand why the isoelectronic species NNO and CO_2 behave so similarly in many instances but not in others. For example, the van der Waals complexes of NNO and CO_2 have similar structures in some cases and yet so different in others. The differences in intermolecular interactions could arise from the differences in the dipole moments, electric quadrupole moments, and polarizabilities of NNO and CO_2.

In the $^{14}N^{14}NO$ molecule where the same cross section can be obtained independently using two different nuclei (we have not carried out the ^{17}O spin relaxation), we provide an example in which it is possible to assess the magnitude of the errors in the determination of such cross sections when competing relaxation mechanisms have to be considered in the analysis, by comparison with the cross sections obtained from the other nucleus which has a single dominant relaxation mechanism.

EXPERIMENT

The gas samples were prepared by condensing a known amount of the gas into a 4 mm×5 cm glass tube held in a liquid nitrogen bath. The tubes were then sealed off from the vacuum line with a torch and placed in an oven maintained at about 400 K to ensure the integrity of the samples at higher temperatures. These tubes just fit into a 5 mm NMR tube and were used without further modification. Gas densities ranged from 7 to 50 amagat (1 amagat is defined as 2.687×10^{19} molecules cm^{-3}) and the nitrogen densities were corrected for uncondensed gas at liquid nitrogen temperature. The estimated error in the N_2 densities is 4% and in the other gases about 2% to 3%. Buffer gases used were Ar, Kr, Xe, N_2, HCl, CO, NNO, CO_2, CH_4, CF_4 and SF_6; all were used as obtained from vendors.

Spin-lattice relaxation times T_1 were measured using the inversion recovery pulse sequence. The inversion-recovery pulse sequence inverts the magnetization with a π pulse, allows the spin system to relax for some delay time τ_D and samples the degree of recovery to equilibrium with a $\pi/2$ pulse. The system is allowed to relax to equilibrium, waiting $\sim5T_1$ before the sequence is repeated. A sufficient number of such cycles provides the desired signal-to-noise ratio (S/N). Seven variable delay times, ranging from $0.2T_1$ to about $1.8T_1$, were used in shuffled order so as to minimize systematic errors. The delay times τ_0 and τ_∞ were added to the beginning and the end of the delay list for an independent check of the stability of experimental conditions. The shortest delay time allowed by the spectrometer, 0.3 μs, was used for τ_0 and a value equal to or greater than $5T_1$ was used for τ_∞. For samples that required more than $\frac{1}{2}$ hour to acquire the desired S/N, the delay list was cycled through a number of times so that more reliable averages were obtained over any variations in the conditions such as temperature fluctuations, changes in probe tuning (and hence errors in the π pulse), etc. over time.

The experiments were run unlocked and the field was shimmed on the ^1H free induction decay (FID) of a methanol or ethylene glycol sample used for temperature determination. For $T<300$ K, the temperature-dependent frequency difference of the methyl and hydroxyl ^1H peaks in methanol was used to calculate the actual temperature of the sample. For $T\geqslant300$ K, the alkyl and hydroxyl proton frequency difference in ethylene glycol was used. Nitrogen boil-off was passed over the heater coil for below room-temperature work and dry air was used for above room-temperature experiments. The temperature of the sample was determined absolutely to within ±0.5 K and was regulated to better than ±0.1 K. Relaxation time measurements were carried out separately for the central and end nitrogens in the NNO molecule for all of the NNO–X systems. The observed relaxation time ranged from 60 to 205 ms for the end nitrogen and 540 ms to 1.3 s for the center nitrogen. The observed triplets were line broadened by about 10 Hz and the single peak intensity was used.

Integration of Bloch's equations leads to intensities proportional to the bulk magnetization along the applied magnetic-field direction which vary with the delay time τ_D as follows:

$$A_D=A_\infty[1-\exp(-\tau_D/T_1)]+A_0\exp(-\tau_D/T_1). \quad (1)$$

The above form accounts for any deviation from the ideal $A_0=-A_\infty$ owing to B_1 (rf) radio frequency field inhomogeneity. Even more importantly, for very short times, Eq. (1) accounts for the finite length of the ideally $\tau_D=0$ delay. Plots of $\ln[(A_\infty-A_D)/(A_\infty-A_0)$ vs τ_D provide a slope of $-1/T_1$.

Figure 1 shows typical inversion recovery experiments for the N_{end} nucleus in a pure sample of $^{14}N^{14}NO$. At a given temperature, the observed T_1 values of the N_{end} and N_{cen} nuclei differ by a factor of about 6 with the end nitrogen having the shorter relaxation time. The range of temperatures for which (T_1/ρ) for ^{14}N relaxation in pure NNO remains independent of density was found to be bounded by 260 K

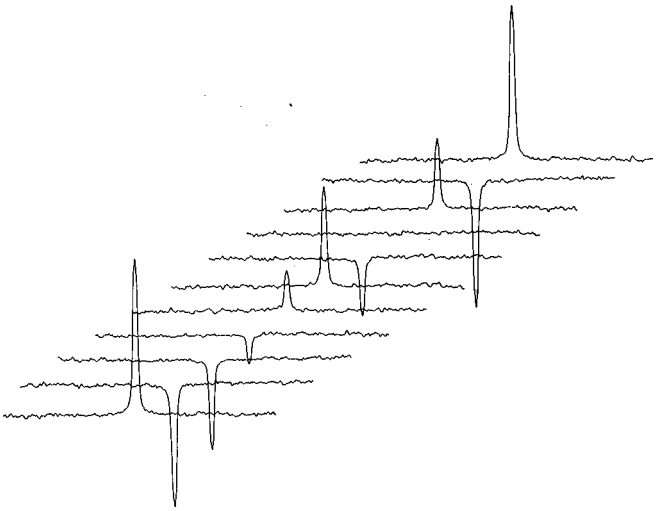

FIG. 1. Typical inversion recovery experiment for the end ^{14}N nucleus in the $^{14}N^{14}NO$ molecule in NNO gas. Delay times from bottom to top are: 0.7, 3×10^{-7}, 0.022, 0.067, 0.135, 0.24, 0.045, 0.09, 0.18, 3×10^{-7}, 0.7 s.

for the densities used (20–40 amagat) and the analysis of the NNO–buffer interactions at lower temperatures requires the extrapolation of the pure NNO results. Although inconsistent variations of T_1 with temperature are not expected below 260 K, lower density pure NNO samples are needed for a more accurate determination of the low temperature ($T<260$ K) T_1 values. The error introduced by this extrapolation is not expected to be much greater than the error associated with the density determination. Condensation of HCl, CO_2, Xe and SF_6 in the samples containing mixtures of NNO with these buffer gases set a lower limit on the temperature range that could be used to obtain relaxation times and collision cross sections for the corresponding NNO–X interactions.

Collision cross sections from relaxation times

The measured relaxation times in the extreme narrowing limit, where the relaxation time is directly proportional to density (the ''linear regime''), provide directly either one of two types of collision cross sections $\sigma_{\theta,2}$ and σ_J when the relaxation is dominated by a single mechanism. For linear molecules, $\sigma_{\theta,2}$ can be obtained directly when the relaxation is dominated by the quadrupolar mechanism. That is[32]

$$\sigma_{\theta,2}=\frac{T_1^Q}{\rho}\frac{3}{160}\frac{(2I+3)}{I^2(2I-1)}\left(\frac{e^2qQ}{\hbar}\right)^2\frac{1}{\langle v\rangle}, \tag{2}$$

can be used with the quadrupolar-dominated relaxation time T_1^Q. For the dipole–dipole relaxation mechanism, there is an analogous relationship with T_1^{DD}

$$\sigma_{\theta,2}=\frac{T_1^{DD}}{\rho}\frac{I(I+1)}{2}\left(\frac{\gamma^2\hbar}{r^3}\right)^2\frac{1}{\langle v\rangle} \tag{3}$$

Values for σ_J can be obtained directly from the spin-rotation-dominated relaxation times in a pure gas of linear molecules using

$$\sigma_J=\frac{T_1^{SR}}{\rho}\frac{4C^2I_0k_BT}{3\hbar^2}\frac{1}{\langle v\rangle}. \tag{4}$$

In our previous work, the relaxation of ^{13}C in CO and CO_2 or ^{15}N in N_2 and NNO were dominated completely by spin rotation and these relaxation times provided σ_j by the above equation.[31,33–35] Similarly, the relaxation of the ^{14}N in N_2 was dominated by quadrupolar relaxation and directly provided $\sigma_{\theta,2}$.[36] In the present work, the ^{14}N relaxation of the end nitrogen in NNO is dominated by the quadrupolar mechanism and provides $\sigma_{\theta,2}$ by Eq. (2).

In a binary mixture, the observed relaxation time $(T_1)^{\rm obs}$ of a nucleus in a probe molecule arises from probe–probe and probe–buffer molecule collisions. Gordon has provided the theoretical basis for the additive nature of the contributions from collisions with two types of molecules.[32] The observed relaxation time can be written as a sum of probe–probe and probe–buffer contributions

$$T_1^\alpha=(T_1^\alpha/\rho)_{pp}\cdot\rho_{\rm probe}+(T_1^\alpha/\rho)_{pb}\cdot\rho_{\rm buffer}. \tag{5}$$

This relation is valid when the full matrix multilevel relaxation is replaced by a single effective relaxation time. Whereas it has been shown that a multiple relaxation time treatment is more appropriate for systems involving molecules with large rotational constants where only two or three rotational levels are populated,[37] this situation does not apply to heavier linear molecules such as N_2 or NNO. The additivity expressed in Eq. (5) applies to binary systems in which many rotational levels of the probe molecule are thermally populated so that the full multilevel relaxation treatment of the relaxation times associated with each of the individual rotational states can be replaced by a single relaxation time. This additivity has been verified experimentally in the spin rotation relaxation studies on various spin$\frac{1}{2}$ nuclei in the gas phase in our laboratory.[31,33–35,38–40] When a single mechanism dominates in a binary mixture, values for the probe–probe contribution to the relaxation must be available from measurements in the pure gas in order to determine the relaxation time due to the unlike interaction; from the latter, the cross section, e.g., $\sigma_{\theta,2}$, can be obtained for the unlike pair of molecules.

Competing relaxation mechanisms in the gas phase

When more than one relaxation mechanism contributes to the observed relaxation time, analysis of the relaxation is made in terms of the relaxation rates $R_1^\alpha=1/T_1^\alpha$,

$$R_1^{\rm obs}=\Sigma_\alpha R_1^\alpha=R_1^Q+R_1^{SR}+R_1^{DD}+\cdots, \tag{6}$$

where each rate corresponds to a different relaxation mechanism, including cross relaxation terms, and the rate for each mechanism is calculated from Eq. (5) by

$$R_1^\alpha=\{(T_1/\rho)_{pp}^\alpha\rho_{\rm probe}+(T_1/\rho)_{pb}^\alpha\rho_{\rm buffer}\}^{-1}. \tag{7}$$

Note that when more than one mechanism has to be considered, $T_1^{\rm obs}$ is no longer directly proportional to the density of the gas. For nuclei with spin $>\frac{1}{2}$ in gas-phase molecules, the quadrupolar rate is almost always the largest. If this rate is significantly larger than the others, the smaller rates can be neglected and the analysis becomes straight forward. One can then compare all possible rates with the rate of the quadrupole mechanism. If however, two or more rates are com-

parable in magnitude, more information is needed to obtain a specific cross section, e.g., $\sigma_{\theta,2}$, for the unlike pair of molecules. For example, when both the quadrupolar and spin-rotation mechanisms contribute to the relaxation, in order to extract the desired $(T_1/\rho)_{pb}^{Q}$ for the quadrupolar mechanism from the observed T_1, independent measures of $(T_1/\rho)_{pp}^{SR}$, $(T_1/\rho)_{pb}^{SR}$, and $(T_1/\rho)_{pp}^{Q}$ are all needed. The value $(T_1/\rho)_{pb}^{Q}$ for the quadrupolar mechanism, so obtained indirectly, can then used to calculate a value for $\sigma_{\theta,2}$ for the probe–buffer collision pair.

Since the quadrupole and dipole–dipole mechanisms involve the same cross section, a ratio of their coupling constants provides a direct measure of their relative importance. For the contribution of the spin-rotation mechanism, the analysis is not as simple. The respective cross sections, σ_J and $\sigma_{\theta,2}$, are different, so that a separate determination of σ_J is needed to compare with the observed rates. From the spin-rotation-dominated studies of spin $I=\frac{1}{2}$ nuclei conducted in our laboratory,[31,33–35,38–40] R_1^{SR} can be determined. However, this would be the rate for the spin $\frac{1}{2}$ nucleus which is of a different mass than the spin $I=1$ nucleus. We need to take into account the mass dependence of the various factors that enter into spin-rotation relaxation. The explicitly mass-dependent factors are the rotational constant and the spin-rotation constant. The ratio of the spin-rotation constants for a linear molecule containing a spin $\frac{1}{2}$ nucleus to that of the same molecule containing the spin 1 nucleus is

$$\frac{C_{\perp}^{[1/2]}}{C_{\perp}^{[1]}}=\frac{g_N^{[1/2]}B_0^{[1/2]}}{g_N^{[1]}B_0^{[1]}}, \tag{8}$$

where the quantities labeled $[\frac{1}{2}]$ (or $[1]$) belong to the spin$\frac{1}{2}$ (or spin 1) nucleus or the molecule containing that nucleus. The explicit mass dependence is in the rotational constant B_0, and the isotope dependence is included in the nuclear g-factor g_N. In addition, there is a mass dependence in the σ_J cross sections, which can only be determined quantitatively by doing classical trajectory calculations of the cross sections for both masses, of course, using the same potential-energy surface. In lieu of this, we can determine semiquantitatively the mass dependence of the σ_J cross sections by a consideration of the trends in the collision efficiencies, $\sigma_J/\pi d_{12}$, found for nine different probe molecules with the same set of ten collision partners.[41] This study showed that a perfectly rough hard spheres model could account for the trends in nearly a hundred different cross sections. In this model, there is a mass dependence in the cross section, contained in the kinematic factor y_{12} such as

$$y_{12}=\left\{\frac{2I_1}{\mu d_{11}^2}+\frac{1}{2}\left(1+\frac{I_1 d_{22}^2}{I_2 d_{11}^2}\right)\right\}^{-1}, \tag{9}$$

where d_{11} is the hard-sphere diameter of the molecule and d_{22} that of its collision partner, the moments of inertia are I_1 and I_2, and μ is the reduced mass of the collision complex. In this paper, we use the ratio of the kinematic factors to take into account the mass dependence in the σ_J cross sections of the spin $\frac{1}{2}$ molecule ($^{15}N^{15}NO$) and the spin 1 molecule ($^{14}N^{14}NO$). The ratio of the relaxation rates is then

$$\frac{R_1^{[1/2]}}{R_1^{[1]}}=\frac{B_0^{[1]}}{B_0^{[1/2]}}\left(\frac{g_N^{[1/2]}}{g_N^{[1]}}\right)^2\left(\frac{\mu^{[1/2]}}{\mu^{[1]}}\right)^{1/2}\frac{y_{12}^{[1/2]}}{y_{12}^{[1]}}. \tag{10}$$

Of course, this treatment is only valid for a nucleus such as hydrogen or nitrogen where both spin 1/2 (^1H and ^{15}N) and spin 1 (^2H and ^{14}N) can exist.

The above analysis depends on a linear relationship between T_1 and ρ. The formation of van der Waals dimers introduces possible complications. In the detailed study of the H_2–Ar system, Lemaire and Armstrong found a (T_1/ρ) that was not constant but passed through a maximum at a particular density.[8] The maximum occurs when

$$\rho_{\max}\langle v\rangle\sigma\approx\omega_{jj}, \tag{11}$$

where σ is the cross section for annihilation of the H_2–Ar van der Waals dimer and ω_{jj} is a measure of the anisotropy-induced splittings in the H_2 rotational levels caused by the formation of the H_2–Ar dimer. The frequencies ω_{jj} are roughly of the order of magnitude of the rotational constant of the dimer. For H_2–Ar, $\rho_{\max}$ occurs at 15 amagat. There were no indications from any of our experiments of a nonlinear dependence of T_1 on density. Estimates of ω_{jj} for the N_2–X and NNO–X dimers from approximate values of the rotational constants of the dimers, estimates of the annihilation cross sections based on geometric cross sections and $\langle v\rangle$ values at 300 K lead to estimates of $\rho_{\max}$. For the NNO–X systems studied here, the values are estimated to be within the following range: $\rho_{\max}\approx 0.2-0.5$ amagat. Thus, there is no expectation for a density-dependent (T_1/ρ) in any of the samples studied here.

RESULTS

Relaxation of the end ^{14}N nucleus in $^{14}N^{14}NO$

In samples of pure $^{14}N^{14}NO$ gas, the observed spin lattice relaxation time constant T_1 for the $^{14}N_{end}$ nucleus is found to vary linearly with density for the density range up to 40 amagat. Since the quadrupolar coupling constant is sufficiently large, $e^2qQ/\hbar=-773.76$ kHz,[42] the relaxation is dominated by the quadrupolar mechanism. In pure $^{14}N^{14}NO$ gas, the ratios of the rates, R_1^{DD}/R_1^{Q} and R_1^{SR}/R_1^{obs}, for the end nitrogen $^{14}N_{end}$ nucleus in NNO are $\sim 1\times 10^{-4}$% and <5%. The values of T_1/ρ for $^{14}N_{end}$ in the pure $^{14}N^{14}NO$ gas are plotted in Fig. 2. The probe–buffer contribution can be readily extracted from the observed T_1 for $^{14}N_{end}$ in mixtures of NNO with other gases, using $(T_1/\rho)_{NNO-NNO}$ from the pure $^{14}N^{14}NO$ gas in Eq. (5). Within the error limits and within the temperature range 260–400 K, the temperature dependence of the characteristic quantities, $(T_1/\rho)_{pp}^{\alpha}$ and $(T_1/\rho)_{pb}^{\alpha}$ are found to be adequately described by a power law

$$(T_1/\rho)[T]=(T_1/\rho)[300\ \text{K}]\cdot(T/300\ \text{K})^n \tag{12}$$

with $n<0$. $(T_1/\rho)[300\ \text{K}]$ for mixed interactions at 300 K are listed in Table I with their respective values of n, determined from fits to the power law. The errors reported are taken from the standard deviations in fitting the data from all samples of various densities to a single straight line for $\ln\{(T_1/\rho)[T]/(T_1/\rho)[300\ \text{K}]\}$ vs $\ln(T/300)$ which provides the

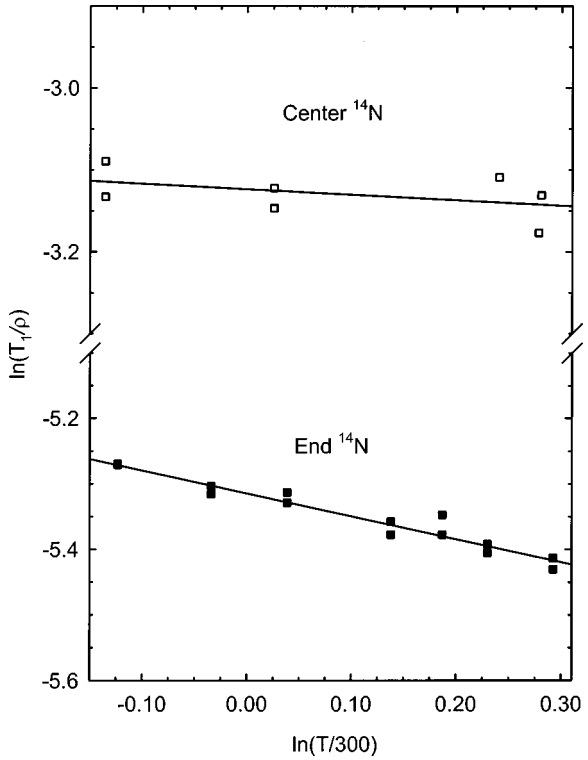

FIG. 2. Temperature dependence of (T_1/ρ) for the end and center ^{14}N nuclei in NNO gas.

value of *n*. Reported standard deviations in $(T_1/\rho)[300\ \mathrm{K}]$ and in *n* are predominantly due to uncertainties in the densities which are expected to be less than 2% or 3% (about 4% for mixtures containing N_2 gas). Comparing Eq. (12) to the T_1 equations, the temperature dependence of the cross sections can be expected to obey a similar power law

$$\sigma_{\theta,2}[T]=\sigma_{\theta,2}[300\ \mathrm{K}]\cdot(T/300\ \mathrm{K})^m, \tag{13}$$

where *m* differs from *n* by the temperature dependence of the mean relative velocity, $\langle v\rangle$, so that $m=n-0.5$. Indeed, this power law adequately describes the $\sigma_{\theta,2}$ values deduced from the experimental relaxation times measured in this work, within the range of temperatures used here.

Relaxation of the center ^{14}N nucleus in ^{14}N^{14}NO

The same samples used for the $^{14}N_{end}$ relaxation measurements were used to study the relaxation of the center nucleus $^{14}N_{cen}$ in the NNO–X mixtures, using only one sample for each mixture in the $^{14}N_{cen}$ relaxation studies for comparison with all samples used for the $^{14}N_{end}$ studies. The relaxation of the $^{14}N_{cen}$ nucleus in the pure $^{14}N^{14}NO$ samples had about a 30% contribution (varying with temperature) from the spin-rotation mechanism. This is due to a combination of a smaller quadrupolar coupling constant $(e^2qQ/\hbar=-267.58\ \mathrm{kHz}$ for $^{14}N_{cen}$ compared with 773.76 kHz for $^{14}N_{end})$[42] and a larger spin-rotation coupling constant: $C_\perp(^{15}N_{cen})=3.35\ \mathrm{kHz}$[35] compared with $C_\perp(^{15}N_{end})=2.48\ \mathrm{kHz}$.[42] Physically, this can be understood by considering that the electric-field gradient at the center nitrogen nucleus should be smaller than that at the end nitrogen nucleus since the center of the molecule has a more symmetric electron distribution than does the end of the molecule.

In pure $^{14}N^{14}NO$ gas, the ratios of the rates, R_1^{DD}/R_1^Q and R_1^{SR}/R_1^{obs}, for the center nitrogen $^{14}N_{cen}$ nucleus are $\sim 2\times10^{-4}$% and 30%. We find the dipole–dipole mechanism can be neglected with respect to the quadrupolar mechanism. The spin-rotation mechanism, however, is competing favorably with the quadrupolar mechanism for the center nitrogen in $^{14}N^{14}NO$. For the end nitrogen in NNO, the quadrupolar mechanism dominates and the observed relaxation rate can be equated with the rate due to the quadrupolar mechanism. For the center ^{14}N in NNO measurements, however, the observed relaxation rate is analyzed as

$$R_1^{obs}=R_1^Q+R_1^{SR}.$$

The rates for each of the two mechanisms were determined from equations of the form of Eq. (7) leading to

$$\{T_1^{obs}\}^{-1}=\{(T_1/\rho)_{pp}^Q\cdot\rho_{probe}+(T_1/\rho)_{pb}^Q\cdot\rho_{buffer}\}^{-1}+\{(T_1/\rho)_{pp}^{SR}\cdot\rho_{probe}+(T_1/\rho)_{pb}^{SR}\cdot\rho_{buffer}\}^{-1}. \tag{14}$$

Note that when two or more mechanisms are included, the dependence of the observed T_1 on density is no longer simple. The density-independent quantities for the spin-rotation mechanism, $(T_1^{SR}/\rho)_{pp}$ and $(T_1^{SR}/\rho)_{pb}$, are obtained from the spin $\frac{1}{2}$ relaxation work in mixtures containing $^{15}N^{15}NO$, converting to the masses appropriate to $^{14}N^{14}NO$ by using the scaling factors discussed earlier. The value of $(T_1/\rho)_{pp}^Q$ for the quadrupolar mechanism of $^{14}N_{cen}$ was obtained from the pure $^{14}N^{14}NO$ gas sample, using the $(T_1/\rho)_{pp}^{SR}$ from $^{15}N_{cen}$ in $^{15}N^{15}NO$ gas. We assign a value of $(T_1/\rho)^{SR}(^{14}N)$ that has been derived from the measured spin-rotation relaxation value of $(T_1/\rho)^{SR}(^{15}N)$ of the earlier ^{15}N relaxation studies in $^{15}N^{15}NO$.[35] For the central ^{14}N nucleus in $^{14}N^{14}NO$ the spin-rotation contribution is then given by

$$(T_1/\rho)_{cen}^{SR}[^{14}N]=(T_1/\rho)_{cen}^{SR}[^{15}N]\cdot\frac{B_0^{[1]}}{B_0^{[1/2]}}\left(\frac{g_N^{[1/2]}}{g_N^{[1]}}\right)^2\left(\frac{\mu^{[1/2]}}{\mu^{[1]}}\right)^{1/2}\frac{y_{12}^{[1/2]}}{y_{12}^{[1]}}. \tag{15}$$

For each sample at each temperature, the spin-rotation contribution is calculated and subtracted out from the observed overall relaxation rate. The remainder is attributed entirely to the quadrupolar mechanism, and is analyzed in exactly the same way as the observed quadrupolar relaxation rate for the end ($^{14}N_{end}$) nucleus. The results of the analysis for the relaxation of the center $^{14}N_{cen}$ nitrogen in NNO–X mixtures are listed in Table I. The uncertainties for the center ^{14}N were estimated from the various errors associated with the spin-rotation contributions that had to be subtracted out. The $(T_1/\rho)_{cen}^Q[^{14}N]$ results for the pure $^{14}N^{14}NO$ samples depend on the previous results of the spin-rotation measurements in $^{15}N^{15}NO$ and are thus expected to have larger errors than for the $^{14}N_{end}$ results in the $^{14}N^{14}NO$-buffer mixtures. On the other hand, the $^{14}N_{cen}$ analysis for the NNO–buffer interac-

TABLE I. Quadrupolar relaxation times for ^{14}N nuclear spins in the NNO molecule with various collision partners. The observed temperature dependence can be described by $(T_1/\rho)[T]$, ms amagat^{-1}=$(T_1/\rho)\times[300\text{ K}]\cdot(T/300\text{ K})^n$.

Collision partner	End nitrogen		Center nitrogen		Temperature range, K
	(T_1/ρ)[300 K]	n	(T_1/ρ)[300 K]	n	
NNO	4.92±0.12	−0.35±0.04	44.0±2.0	−0.07±0.16	265–400
CH_4	4.04±0.11	−0.29±0.03	40.8±1.0	−0.05±0.10	230–400
N_2	3.18±0.15	−0.27±0.06	24.1±0.5	−0.29±0.10	230–400
CO	3.47±0.15	−0.32±0.04	30.4±1.6	−0.08±0.20	230–400
Ar	3.18±0.06	−0.23±0.02	27.3±0.6	−0.06±0.08	230–400
HCl	4.34±0.09	−0.45±0.04	39.6±2.2	0.00±0.32	280–400
CO_2	4.91±0.24	−0.43±0.07	40.6±2.0	0.05±0.28	280–400
CF_4	4.52±0.13	−0.19±0.03	39.7±1.8	−0.07±0.20	230–400
Kr	3.74±0.11	−0.30±0.03	32.6±1.0	0.05±0.14	230–400
Xe	4.06±0.13	−0.27±0.05	38.5±2.6	0.18±0.36	260–400
SF_6	5.22±0.14	−0.16±0.06	46.4±2.4	0.07±0.42	290–400

tions depends not only on two sets of spin-rotation relaxation measurements in ^{15}N^{15}NO-containing samples, but also on the results for $^{14}N_{cen}$ relaxation in the pure ^{14}N^{14}NO samples. Thus, the results for the center nitrogen nucleus in the NNO–buffer mixtures have additional, substantial errors not reflected in the standard deviations obtained from analysis of the data. Furthermore, there are unknown errors associated with the assumed mass-dependence of σ_J in going from ^{15}N^{15}NO to ^{14}N^{14}NO. Based on a ''worst case'' where the spin-rotation parameters (T_1/ρ) and n were increased by twice their respective standard deviations, the cross sections at 300 K and the temperature dependence derived from $^{14}N_{cen}$ relaxation measurements can be brought into agreement with the results for the $^{14}N_{end}$ relaxation measurements. The temperature dependence of the (T_1/ρ) for the end and central nitrogens should be identical. They are not. The cross section $\sigma_{\theta,2}$ is a molecular property which can be determined from relaxation studies of any spin-containing nucleus within the molecule. Therefore, the cross sections obtained from the central ^{14}N measurements in ^{14}N^{14}NO should be identical to the cross sections obtained from the end ^{14}N in the same molecule in the same sample. They are not. In Figs. 3 and 4 we observe the discrepancy between the $^{14}N_{end}$ direct measurements and the $^{14}N_{cen}$ quadrupolar part obtained by the subtraction described above. By plotting the cross sections $\sigma_{\theta,2}$ derived from both $^{14}N_{end}$ and $^{14}N_{cen}$ measurements in the same figure, we can observe directly the errors associated with separating the two contributing relaxation mechanisms for the $^{14}N_{cen}$ nucleus. The apparent temperature dependence for the center ^{14}N is too flat, which reflects having subtracted out too much spin-rotation contribution. The temperature dependence of $(T_1/\rho)^{SR}$ is steeper than that of $(T_1/\rho)^Q$ because of the explicit dependence of the former on $\langle J^2\rangle$, which (classically) is $2I_0k_BT/\hbar^2$ for linear molecules, apart from the temperature dependence in the cross section itself. Therefore, any errors in subtracting out the spin-rotation contribution have important consequences in the temperature dependence of the remainder that is attributed to the quadrupolar contributions.

Thus, we have used a treatment of multiple relaxation mechanisms in the gas phase to obtain collision cross sections, however, attention must be directed towards the uncertainties associated with the experimental results of the contributing mechanisms. In Table I, the central nitrogen $(T_1/\rho)^Q$ have systematic errors due to this and are, therefore, considered less reliable. The strong temperature dependence of the spin-rotation mechanism leaves a large systematic error in the temperature dependence of the remainder which is attributed to quadrupolar relaxation. Thus, all the succeeding tables (Tables II and III) and discussions above are based on the data arising from the end ^{14}N.

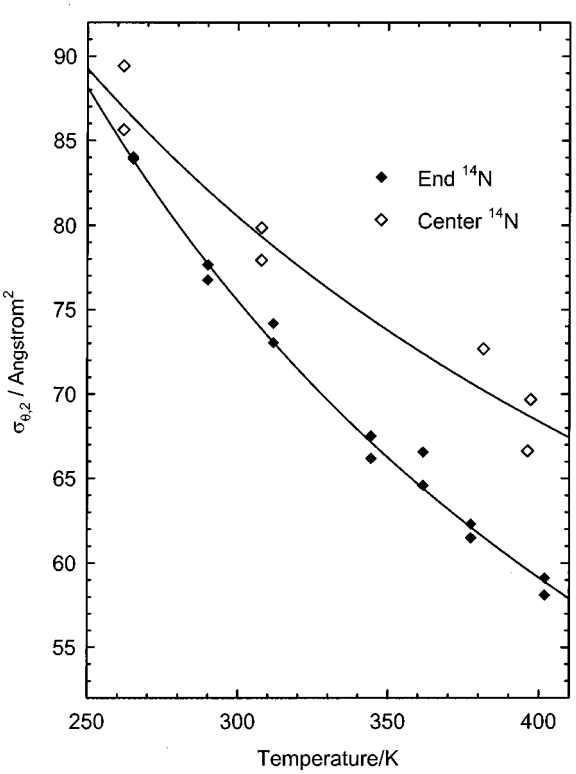

FIG. 3. The cross section $\sigma_{\theta,2}$ for the NNO molecule in collisions with NNO. The data from the center ^{14}N nucleus have systematic errors as discussed in the text.

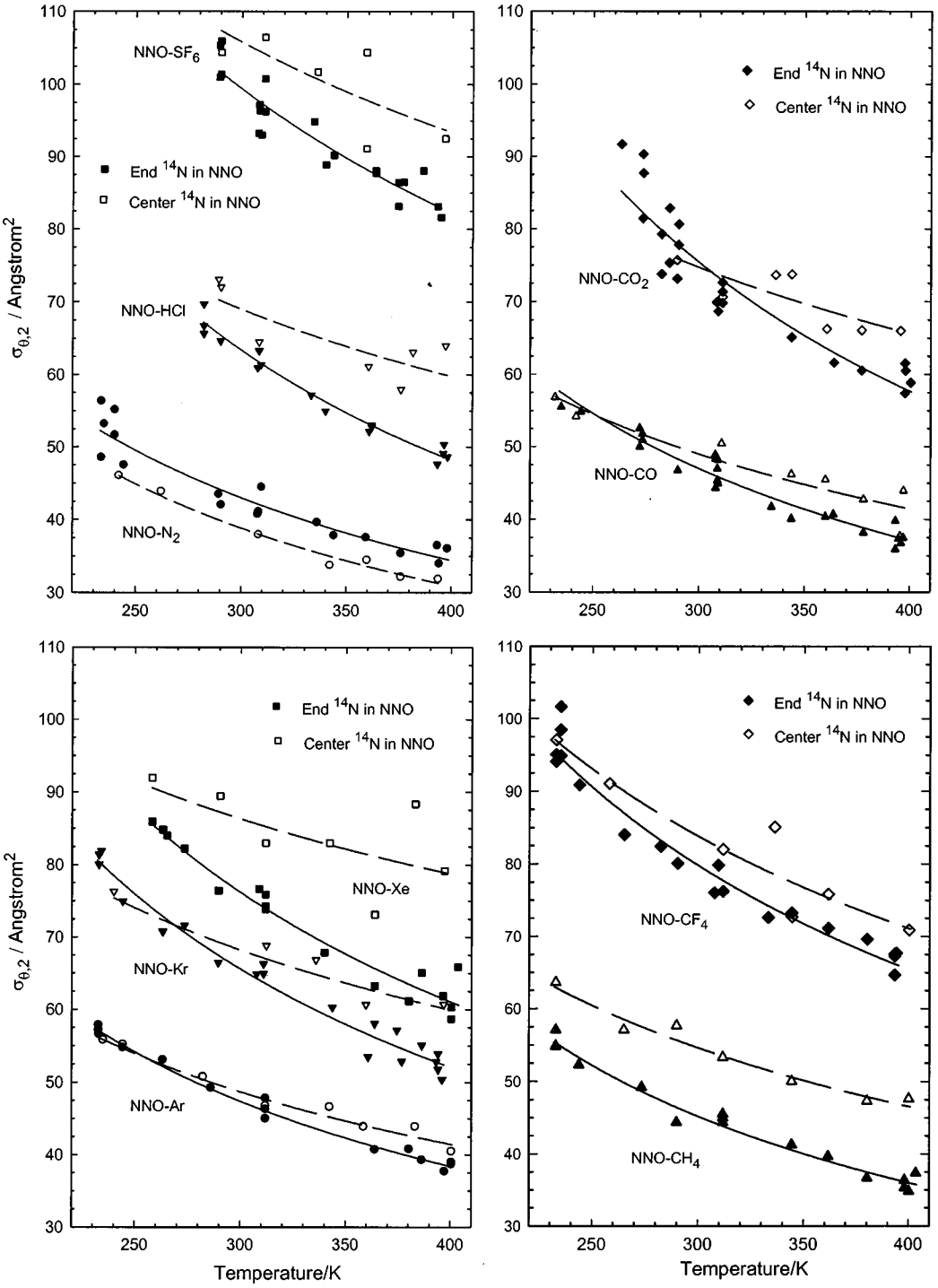

FIG. 4. The cross section $\sigma_{\theta,2}$ for the NNO molecule in collisions with buffer gases. The data from the center ^{14}N nucleus have systematic errors as discussed in the text.

DISCUSSION

Trends in the cross sections

As can be seen in Table II, the values for $\sigma_{\theta,2}(300\ \mathrm{K})$ tend to increase with the size of the collision partner, with the exception of HCl. The temperature dependence does not follow a similar trend with size. All have a negative power dependence on temperature and the magnitude of the temperature dependence appears to increase with increasing contributions to the interaction energy from the electric moments (e.g., dipole, quadrupole) and of the polarizability of the buffer molecule, with the possible exception of Xe. Such a trend may be indicative of a dependence of m on the attractive part of the relevant PES, as illustrated in Fig. 5(a) where $|m|$, more explicitly $|m_\theta|$, is plotted against the angle-averaged well depth ϵ for NNO–X. Estimates of the latter have been taken from Ref. 43. Although the scatter is large, a general trend of increasing $|m_\theta|$ with increasing well depth for the pair potential is observed. The correlation is made

TABLE II. Relaxation cross sections (Å^2) for the rotational angular momentum vector in NNO molecule with various collision partners. The temperature dependence can be described by $\sigma[T]=\sigma[300\ \mathrm{K}]\cdot(T/300\ \mathrm{K})^m$.

Collision partner	*a*		*b*		ratio
	$\sigma_{\theta,2}$[300 K]	*m*	σ_J[300 K]	*m*	$\sigma_{\theta,2}/\sigma_J$
NNO	75.5±1.9	−0.85±0.04	59.3±1.1	−0.91±0.01	1.27
CH_4	45.2±1.3	−0.79±0.03	27.1±2.0[c]	−0.47±0.17[c]	1.67
N_2	43.0±1.9	−0.77±0.06	29.4±1.7[c]	−0.68±0.11[c]	1.46
CO	47.0±1.6	−0.82±0.04	33.1±1.3	−0.81±0.05	1.42
Ar	47.4±0.9	−0.73±0.02	37.7±2.2	−0.86±0.06	1.26
HCl	63.4±1.3	−0.95±0.04	51.9±2.2[c]	−1.06±0.11[c]	1.22
CO_2	75.4±3.7	−0.93±0.07	59.8±3.9	−0.94±0.11	1.26
CF_4	79.8±2.1	−0.69±0.03	71.7±3.1	−0.87±0.07	1.11
Kr	65.6±2.0	−0.80±0.03	55.6±4.8	−0.96±0.11	1.18
Xe	76.2±2.6	−0.77±0.05	64.6±4.7	−0.92±0.13	1.18
SF_6	99.4±2.8	−0.66±0.06	103.6±5.8[c]	−1.29±0.17[c]	0.96

[a]Based on the relaxation times of the end ^{14}N nucleus in $^{14}N^{14}NO$ this work.
[b]Based on the relaxation times of both ^{15}N nuclei in $^{15}N^{15}NO$ (Ref. 35).
[c]Based on the relaxation times of both ^{15}N nuclei in $^{15}N^{15}NO$ (Ref. 53).

more evident in Fig. 5(b), which shows the correlation of the temperature dependence of the σ_J for various probes listed in the legend, by using *averages* of $|m_J|$ and of ϵ over the same set of collision partners as in Fig. 5(a). All the values of $|m_\theta|$ and ϵ for NNO–X are displayed for individual collision partners X listed in Fig. 5(a), whereas all the values of $|m_J|$ and ϵ for NNO–X are displayed as a single point for the NNO probe, for comparison with other probes listed in Fig. 5(b).

The cross sections have an implicit dependence on the size of the interacting molecules so that values of $\sigma_{\theta,2}$ for $^{14}N^{14}NO$–SF_6 are the largest among the collision pairs. To properly compare the relative magnitudes of the cross sections for various interaction pairs, the collision efficiencies $b_{\theta,2}=(\sigma_{\theta,2}/\sigma_{\mathrm{geom}})$ are used to account for size differences among the collision partners. Here, the geometric cross section σ_{geom} is taken to be πr_0^2, where r_0 is the average distance at which the isotropic average potential function is zero. Table III lists the collision efficiencies for the NNO–X systems. The values for the spin-rotation collision efficiencies $b_J=(\sigma_J/\sigma_{\mathrm{geom}})$ from Ref. 35 are also listed in Table III. Clearly, both sets follow a similar trend with increasing values of the efficiencies. The efficiencies do not follow a linear dependence on the electric dipole polarizability of the collision partner. The systems involving molecules with large electric moments, such as HCl and CO_2 (and NNO itself), have larger collision efficiencies than would be expected based on a polarizability argument. The position of SF_6 in the ordering of the efficiencies suggests the possibility that dependence of σ_J and $\sigma_{\theta,2}$ on mass may not be the same. It has been found by Nielsen and Gordon[1] that σ_J, more so than $\sigma_{\theta,2}$, includes contributions from collisions in which the magnitude, not just the direction of the molecular angular momentum vector **J** of the probe molecule is changed. For these contributions, a heavier collision partner can lead to a greater transfer of translational energy to rotational energy. The spin-rotation collision efficiencies cover a larger range than do those for $\sigma_{\theta,2}$; the b_J range from 0.626 to 1.64 whereas $b_{\theta,2}$ range from 1.02 to 1.75. The uncertainty in the cross sections, however, prevents any meaningful discussion of these ranges.

Instead of the ranges in collision efficiencies, the ratio of $\sigma_{\theta,2}$ to σ_J can provide insight into the differences and similarities of the two cross sections. The cross-section ratios are listed in Table II for NNO with eleven collision partners, including NNO. For all but SF_6, the ratio $\sigma_{\theta,2}/\sigma_J$ is greater than unity and nearly constant, indicating the importance of the nature of the probe molecule, NNO, with an average value of about 1.2 (with the exception of CH_4, N_2, and CO). The average is 1.3±0.2 for all pairs. It may be assumed that the effects of the collision partner are partly washed out by taking the ratio of the cross sections except for the fact that the ratios decrease with increasing polarizability of buffer. The change in $\sigma_{\theta,2}/\sigma_J$ with partner polarizability is small in going from one buffer to another, but the difference between the two extremes (about 0.5) is in excess of the associated

TABLE III. Collision efficiencies for changes in the rotational angular momentum vector of NNO molecule with various collision partners.

Collision partner	σ_{geom}[a] Å^2	$\sigma_{\theta,2}/\sigma_{\mathrm{geom}}$	$\sigma_J/\sigma_{\mathrm{geom}}$
NNO	43.08	1.75	1.38
CH_4	43.29	1.04	0.626
N_2	42.24	1.02	0.696
CO	41.81	1.12	0.792
Ar	38.53	1.23	0.978
HCl	38.95	1.63	1.33
CO_2	43.85	1.72	1.36
CF_4	53.87	1.48	1.33
Kr	41.67	1.57	1.33
Xe	45.60	1.67	1.42
SF_6	63.00	1.58	1.64

[a]The geometric cross section is defined as $\sigma_{\mathrm{geom}}=\pi r_0^2$, where r_0 values were taken as arithmetic means of the r_0 for like pairs. The latter were taken from the pair potentials based on corresponding states, from Ref. 43, except for r_0(CO–CO)=3.592 Å (Ref. 56) and r_0(HCl–HCl)=3.339 Å (Ref. 57).

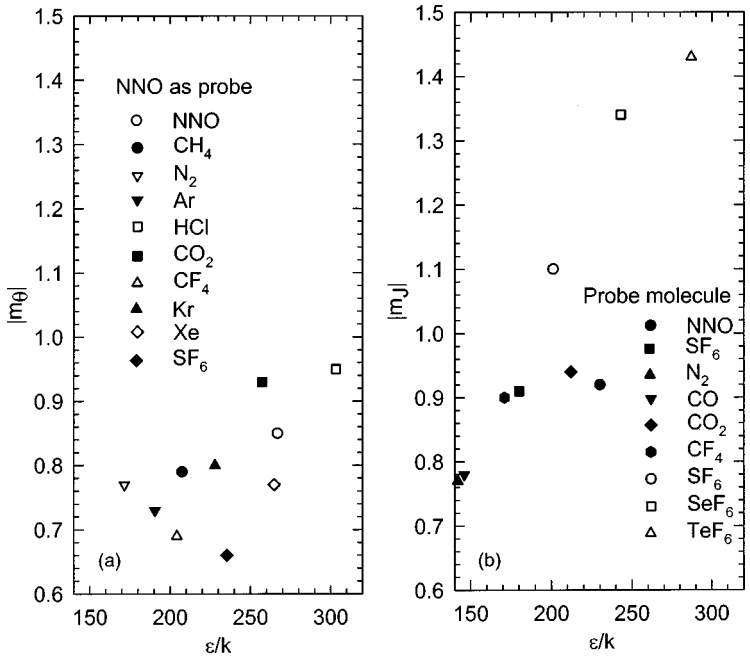

FIG. 5. Correlation of the temperature dependence of the NMR cross sections with the isotropic well depth (ϵ/k, K). The parameter m_θ expresses the (uniformly negative) power law dependence found experimentally, as in $\sigma_{\theta,2}[T]=\sigma_{\theta,2}[300\ \mathrm{K}]\cdot(T/300\ \mathrm{K})^{m}_{\theta}$. In (a) $|m_\theta|$ for NNO with various collision partners listed in the legend from this work correlates weakly with the isotropic well depth (ϵ/k, K) for the pair NNO–X. On the other hand, (b) shows the correlation of the temperature dependence of the NMR cross sections σ_J for various probes listed in the legend, using averages of $|m_J|$ and of ϵ over the same collision partners as in (a), from Ref. 58.

uncertainty. Thus, the two NMR cross sections may indeed depend differently on the collision partner polarizability and hence on the attractive potential. Theoretical calculations of $\sigma_{\theta,2}$ and σ_J are required for a quantitative understanding of these cross sections. Worth noting is that in the N_2–X system, the $\sigma_{\theta,2}/\sigma_J$ ratios have a somewhat narrower range of values (1.92–2.3)[36] and so do the ^{2}H in CD_4–X systems (2.1–2.5).[44]

The $\sigma_{\theta,2}$ cross section is a property of the molecule and its collision partner. Any nucleus in the same molecule (provided only that it relaxes by either dipolar or quadrupolar mechanism or both) may in principle be used to determine this cross section. Therefore, we fully expect the same $\sigma_{\theta,2}$ cross section to result from measurements of relaxation of the central ^{14}N nucleus as for the end ^{14}N nucleus. The end ^{14}N relaxation is completely dominated by the quadrupolar mechanism, the spin rotation and other mechanisms providing negligible contributions. On the other hand, for the central ^{14}N nucleus in NNO–X mixtures about 30% of the observed relaxation rate is due to the spin-rotation mechanism. Thus, in order to obtain values for $\sigma_{\theta,2}$ from the T_1 measurements of the central ^{14}N in these mixtures, it was necessary to derive the spin-rotation contributions in $^{14}N_{cen}$ in $^{14}N^{14}NO$ from measurements of the $^{15}N_{cen}$ relaxation in $^{15}N^{15}NO$. The errors associated with subtracting out a large contribution arising from the highly temperature-dependent spin-rotation relaxation prohibits determination of accurate values for $\sigma_{\theta,2}$ in the NNO–X systems from the central nitrogen. In Table I the error bars for the central nitrogen do not include the systematic errors associated with this subtraction. (In contrast, for ^{2}H relaxation in CD_4 in gas mixtures, the percentage of spin-rotation is about eight and the separation is more favorable.[44]) These results illustrate the difficulties associated with extracting effective cross sections from spin-relaxation data where competing mechanisms exist. In this case, we have an independent probe ($^{14}N_{end}$) to test the reliability of separating the two relaxation contributions. For this reason, only the results for the end nitrogen have been used in the preceding discussion.

Comparison with reorientation models

In a dilute gas, the cross sections $\sigma_{\theta,2}$ and σ_J can be calculated from first principles.[3] In the liquid phase, the complexity of molecular interactions prohibits a simple description of the dynamics. The persistence of a molecular rotational angular momentum is not as unambiguous as in the dilute gas. Nevertheless, for a given physical model of dynamics in the liquid, it is possible to define correlation functions that characterize the rotational motion of molecules in terms of the angular momentum vector, the angular velocity, and various Legendre functions of the orientation of the molecular inertial axes. For a given molecule in a fluid, the correlation times τ_J, $\tau_{\theta,1}$, and $\tau_{\theta,2}$ are related to each other by the nature of the model, and the reduced correlation times τ^*_J, $\tau_{\theta,1}$, and $\tau^*_{\theta,2}$ are defined as follows:

$$\tau^*_J=[(I_0/k_BT)^{1/2}]^{-1}\int \langle \mathbf{J}(0)\cdot\mathbf{J}(t)\rangle/\langle \mathbf{J}(0)\cdot\mathbf{J}(0)\rangle dt,$$

$$\tau^*_{\theta,1}=[(I_0/k_BT)^{1/2}]^{-1}\int \langle P_1(\mathbf{u}(0)\cdot\mathbf{u}(t))\rangle/ \langle P_1(\mathbf{u}(0)\cdot\mathbf{u}(0))\rangle dt, \tag{16}$$

$$\tau^*_{\theta,2}=[(I_0/k_BT)^{1/2}]^{-1}\int \langle P_2(\mathbf{u}(0)\cdot\mathbf{u}(t))\rangle/ \langle P_2(\mathbf{u}(0)\cdot\mathbf{u}(0))\rangle dt,$$

where $(k_BT/I_0)^{1/2}$ is the average time for a classical rotor, in thermal equilibrium at temperature T, to rotate by an angle of one radian. In the liquid phase, where $\tau^*_J \ll 1$, the various models (the extended diffusion model,[45] Ivanov model,[46,47] Langevin model,[48] and friction model[49]) all predict $(\tau^*_{\theta,2}/\tau^*_J)=\frac{1}{6}$, which agrees with the Hubbard relation,[50] as predicted by Debye's rotational diffusion model that pro-

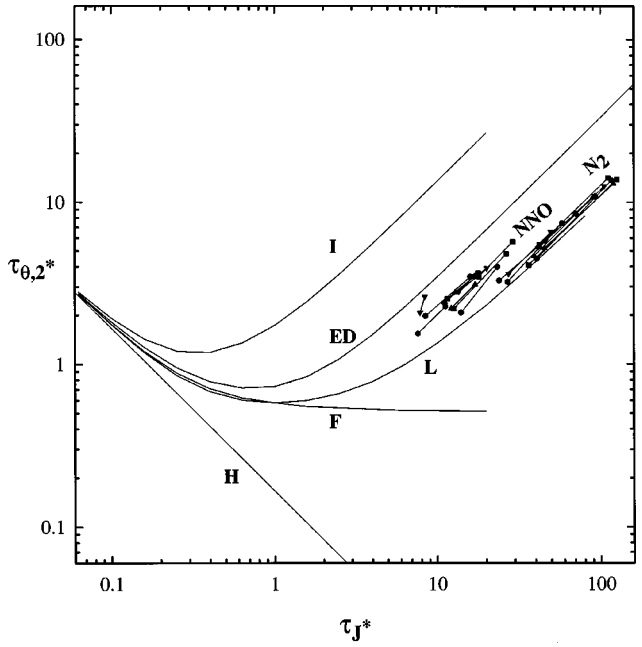

FIG. 6. Comparison of the correlation times for NNO with predictions of various models for molecular reorientation. Included also are N_2 (Ref. 53) for comparison.

vides an accurate description of molecular reorientation in dense fluids at low temperatures.[51] Powles and Rickayzen have shown that the various models can be distinguished from one another when $\tau_J^* \gg 1$; in particular, in the limit of very large τ_J^* (in the dilute gas), the ratio $(\tau_{\theta,2}^*/\tau_J^*)$ approaches $\frac{1}{3}$ for the extended model, $\frac{4}{3}$ for the Ivanov model and $1/10.05\cdots$ for the Langevin model.[52] The friction model leads to a constant value of 5.14 for $\tau_{\theta,2}^*$, independent of τ_J^*. The predictions from the various reorientation models are presented in Fig. 6. The reduced correlation times τ_J^* and $\tau_{\theta,2}^*$ to be compared with these models were calculated from the respective cross sections (measured in this work and in Refs. 35 and 53) using

$$\tau_J^* = [\rho \langle v \rangle \sigma_J (I_0/k_B T)^{1/2}]^{-1} \quad \text{from spin-rotation relaxation}$$

and

$$\tau_{\theta,2}^* = [4\rho \langle v \rangle \sigma_{\theta,2} (I_0/k_B T)^{1/2}]^{-1}$$

$$\text{from quadrupolar relaxation,} \qquad (17)$$

where I_0 is the moment of inertia of NNO. Comparison is made between the correlation times calculated from the cross sections and the predictions from various reorientation models in Fig. 6. The plot of $\tau_{\theta,2}^*$ vs τ_J^* for the NNO–X systems (this work) produces values in a region between the extended-J diffusion and Langevin models, and coincides with the results for ClF.[54] Also included in Fig. 6 are the results for N_2.[36] The gas-phase results for the N_2–X systems coincide with a narrow band running parallel and close to the Langevin model. The extended diffusion (ED) model assumes free rotational motion interrupted by instantaneous, uncorrelated binary collisions which randomize the rotational angular momentum vector of the probe molecule.[45] The differences in the correlation times may be related to the energies of the rotational states in each of the probe molecules. The separation of the rotation states in NNO is smaller than the separations in rotational energies for N_2 which would indicate that NNO can experience more effective inelastic collisions than N_2. This is consistent with the smaller values for τ_J^* (greater frequency of effective collisions and greater σ_J) for the NNO systems than in the N_2 systems. In fact, in comparing the collision efficiencies from an N_2–X system to the corresponding NNO–X system, the spin-rotation efficiency b_J increases by a factor of roughly 3, whereas little change is observed in the quadrupolar efficiency $b_{\theta,2} = \sigma_{\theta,2}/\sigma_{\text{geom}}$.

CONCLUSIONS

This is the second report of $\sigma_{\theta,2}$ cross sections determined from NMR spin-relaxation measurements as a function of temperature for a variety of systems. The earlier work on the relaxation of the ^{14}N nucleus in the N_2–X mixtures[36] and the present one of the $^{14}N_{\text{end}}$ nucleus in NNO–X mixtures have shown that the relaxation is dominated by the quadrupolar relaxation mechanism, so that values for $\sigma_{\theta,2}$ could be calculated directly from the observed relaxation times. The values of $\sigma_{\theta,2}$ differ depending on the nature of the interacting molecules but all show a negative power dependence on temperature. Comparisons with σ_J data has shown that the ratio $\sigma_{\theta,2}/\sigma_J$ is relatively insensitive to the identity of the collision partners. We found that the ratio $\sigma_{\theta,2}/\sigma_J$ is about 2.1 for N_2–X[36] and 1.3 for the NNO–X systems (this work) and the ratio for the CD_4 systems is $\sim$2.3, nearly independent of the collision partner.[44] Clearly, this indicates the overwhelming importance of the nature of the probe molecule for these two types of cross sections.

The linear rotor–atom systems considered here provide encouraging prospects for calculating NMR cross sections from proposed potential-energy surfaces. It has been demonstrated in the H_2–He,[4–6] H_2–Ne,[7] H_2–Ar,[8] D_2,HD–Ar,[59,60] CO_2–Ar,[55] N_2–Ar,[9] and N_2–Kr[10,11] systems that the NMR relaxation times provide stringent tests of the anisotropy of the potential surface. While the virial coefficient, diffusion coefficient and mixture viscosity data provide the usual means by which potential-energy surfaces can be tested, it has been shown in these systems that the magnitudes and the temperature dependences of the NMR cross sections differentiate amongst the various surfaces. Although completely reliable surfaces are not yet available, the $\sigma_{\theta,2}$ cross sections reported here for $^{14}N^{14}NO$ combined with the σ_J cross sections reported earlier for $^{15}N^{15}NO$[35] in collisions with various molecules will be invaluable for testing the anisotropies of any proposed potential functions involving the interaction of the NNO molecule with other molecules (see the following paper, for example).

[1] W. B. Nielsen and R. G. Gordon, J. Chem. Phys. **58**, 4131 (1973); **58**, 4149 (1973).
[2] F. R. W. McCourt, J. J. M. Beenakker, W. E. Köhler, and I. Kuščer, *Nonequilibrium Phenomena in Polyatomic Gases Part I. The Dilute Gas* (Oxford University Press, Oxford, 1990), Vol. 1.
[3] F. R. W. McCourt, J. J. M. Beenakker, W. E. Köhler, and I. Kuščer, *Nonequilibrium Phenomena in Polyatomic Gases Part II. Cross Sections,*

Scattering and Rarefied Gases (Oxford University Press, Oxford, 1990), Vol. 2.
[4] C. Lemaire, R. L. Armstrong, and F. R. W. McCourt, J. Chem. Phys. **81**, 5275 (1984).
[5] R. L. Armstrong, M. Bogdan, K. R. Jeffrey, C. Bissonnette, and F. R. W. McCourt, J. Chem. Phys. **99**, 5754 (1993).
[6] R. S. Wagner, R. L. Armstrong, C. Bissonnette, and F. R. W. McCourt, J. Chem. Phys. **92**, 5907 (1990).
[7] R. S. Wagner, R. L. Armstrong, C. Lemaire, and F. R. W. McCourt, J. Chem. Phys. **84**, 1137 (1986).
[8] C. Lemaire and R. L. Armstrong, Can. J. Phys. **63**, 179 (1985).
[9] L. Beneventi, P. Casavecchia, G. G. Volpi, C. C. K. Wong, and F. R. W. McCourt, J. Chem. Phys. **98**, 7926 (1993).
[10] F. R. W. McCourt, M. A. ter Horst, and C. J. Jameson, J. Chem. Phys. **102**, 5752 (1995).
[11] M. A. ter Horst and C. J. Jameson, J. Chem. Phys. **102**, 4431 (1995).
[12] C. H. Joyner, T. A. Dixon, F. A. Baiocchi, and W. Klemperer, J. Chem. Phys. **75**, 5285 (1981).
[13] C. Dutton, A. Sazonov, and R. A. Beaudet, J. Phys. Chem. **100**, 17772 (1996).
[14] Y. J. Xu and A. R. W. McKellar, J. Mol. Spectrosc. **180**, 164 (1996).
[15] H. B. Qian and B. J. Howard, J. Mol. Spectrosc. **184**, 156 (1997).
[16] R. W. Randall, T. R. Dyke, B. J. Howard, Faraday Discuss. Chem. Soc. **86**, 21 (1988).
[17] Y. P. Zeng, S. W. Sharpe, D. Reifschneider, C. Wittig, and R. A. Beaudet, J. Chem. Phys. **93**, 183 (1990).
[18] J. Hodge, G. D. Hayman, T. R. Dyke, and B. J. Howard, J. Chem. Soc., Faraday Trans. 2 **82**, 1137 (1986).
[19] T. A. Hu, E. L. Chappell, and S. W. Sharpe, J. Chem. Phys. **98**, 6162 (1993).
[20] B. J. Howard, *Structure and Dynamics of Weakly Bonded Molecular Complexes*, edited by A. Weber, NATO ASI Series, Vol. 212 (Reidel, Dordrecht, 1987), pp. 69–84.
[21] H. B. Qian, W. A. Herrebout, and B. J. Howard, Mol. Phys. **91**, 689 (1997).
[22] Z. S. Huang and R. E. Miller, J. Chem. Phys. **89**, 5408 (1988).
[23] D. J. Pauley, M. A. Roehig, L. Adamowicz, J. C. Shea, S. T. Haubrich, and S. G. Kukolich, J. Chem. Phys. **94**, 899 (1991).
[24] H. O. Leung, D. Gangwani, and J. U. Grabow, J. Mol. Spectrosc. **184**, 106 (1997).
[25] H. O. Leung, J. Chem. Phys. **108**, 3955 (1998).
[26] L. Berreby and E. Dayan, Mol. Phys. **48**, 581 (1983).
[27] C. Dreyfus and J. Cartigny, J. Chem. Phys. **80**, 5388 (1984).
[28] L. Berreby and E. Dayan, Chem. Phys. Lett. **243**, 85 (1995).
[29] C. Dreyfus, C. Breuillard, and Y. Guissani, Mol. Phys. **62**, 1275 (1987).
[30] H. W. Nicolaisen and H. Maeder, Mol. Phys. **73**, 349 (1991).
[31] C. J. Jameson, N. C. Smith, and K. Jackowski, J. Chem. Phys. **86**, 2717 (1987).
[32] R. G. Gordon, J. Chem. Phys. **44**, 228 (1965).
[33] C. J. Jameson, A. K. Jameson, and K. Buchi, J. Chem. Phys. **85**, 697 (1986).
[34] C. J. Jameson, A. K. Jameson, and N. C. Smith, J. Chem. Phys. **86**, 6833 (1987).
[35] C. J. Jameson, A. K. Jameson, J. K. Hwang, and N. C. Smith, J. Chem. Phys. **89**, 5642 (1988).
[36] C. J. Jameson, A. K. Jameson, and M. A. ter Horst, J. Chem. Phys. **95**, 5799 (1991).
[37] C. L. Lemaire and R. L. Armstrong, J. Chem. Phys. **81**, 1626 (1984).
[38] C. J. Jameson and A. K. Jameson, J. Chem. Phys. **88**, 7448 (1988).
[39] C. J. Jameson and A. K. Jameson, J. Chem. Phys. **89**, 866 (1988).
[40] C. J. Jameson, A. K. Jameson, N. C. Smith, J. K. Hwang, and T. Zia, J. Phys. Chem. **95**, 1092 (1991).
[41] C. J. Jameson and A. K. Jameson, J. Chem. Phys. **93**, 3237 (1990).
[42] J. M. L. J. Reinartz, W. L. Meertz, and A. Dymanus, Chem. Phys. **341**, 19 (1976).
[43] G. C. Maitland, M. Rigby, E. B. Smith, and W. A. Wakeham, *Intermolecular Forces: Their Origin and Determination* (Clarendon, Oxford, 1981), Table A3.2
[44] C. J. Jameson, M. A. ter Horst, and A. K. Jameson (to be published).
[45] R. G. Gordon, J. Chem. Phys. **44**, 1830 (1966).
[46] E. N. Ivanov, Sov. Phys. JETP **18**, 1041 (1964).
[47] E. Kluk, Mol. Phys. **30**, 1723 (1975).
[48] J. McConnell, *The Theory of Nuclear Magnetic Relaxation in Liquids* (Cambridge University Press, New York, 1987).
[49] E. Kluk and J. G. Powles, Mol. Phys. **30**, 1109 (1975).
[50] P. S. Hubbard, Phys. Rev. A **9**, 481 (1963).
[51] R. E. D. McClung, J. Chem. Phys. **51**, 3842 (1969).
[52] J. G. Powles and G. Rickayzen, Mol. Phys. **33**, 1207 (1977).
[53] M. A. ter Horst, Ph.D. thesis, University of Illinois at Chicago, 1994.
[54] K. T. Gillen, D. C. Douglass, and J. E. Griffiths, J. Chem. Phys. **69**, 461 (1978).
[55] M. A. ter Horst and C. J. Jameson, J. Chem. Phys. **105**, 6787 (1996).
[56] R. D. Trengove, J. L. Robjohns, and P. J. Dunlop, Ber. Bunsenges. Phys. Chem. **88**, 450 (1984).
[57] A. F. Turfa and R. A. Marcus, J. Chem. Phys. **70**, 3035 (1979).
[58] C. J. Jameson, A. K. Jameson, and R. Terry, J. Phys. Chem. **95**, 2982 (1991).
[59] H. Sabzyan, W. P. Power, and F. R. W. McCourt, J. Chem. Phys. **108**, 2361 (1998).
[60] H. Sabzyan, W. P. Power, and F. R. W. McCourt, J. Chem. Phys. **108**, 6170 (1998).